Al-Nahrain Journal of Science
ANJS, Vol. 28(3), September, 2025, pp. 111 – 118

Photo-Responsive Evaluation of Solution-Processed Self-Driven Visible-Blind NiO/ZnO/FTO Photodetector

Mohammed Ali H. Al-Beayaty[1,*], Abdal Kareem A. Dhahir[2], Maryam Abdulghafor Ahmed[1]

[1]Department of Renewable Energy, College of Energy and Environmental Sciences, Al-Karkh University of Science, Baghdad, Iraq.
[2] University of Information Technology and Communication, Baghdad, Iraq

Article's Information

Received: 28.04.2025
Accepted: 03.06.2025
Published: 15.09.2025

Keywords:
Photodetector,
NiO/ZnO/FTO,
solution-processed,
self-driven,
visible-blind

Abstract

In this article, the fabrication procedure of solution-processed NiO/ZnO/FTO heterostructure is systematically elucidated for self-driven visible-blind photodetector application. In detail, the opto-electrical analysis was investigated under multi-illumination wavelength of 375 nm, through which a linear dependency between the photocurrent (I_{ph}) and the incident intensity was perceived along a close to unity Pearson correlation coefficient ($R^2 \approx 1$). The proposed heterojunction (p-NiO/n-ZnO) exhibited short-circuit current and open-circuit voltage of 4 μA and 0.8 V, which in turn validates the self-powered feature of the proposed geometry. The attained photo-responsivity (R_λ) and photo-detectivity (D^*) exhibited values of 25.6 mA/W and 16.3×10^{12} Jones, respectively, under light intensity of 17 mW/cm2. This was noticed along with considerable (R_λ) reduction near the visible light region. In conjunction, p-NiO/n-ZnO heterostructure demonstrated UV/vis rejection ratio ($\lambda_{375}/\lambda_{625}$) of 572; other considered geometries (NiO/FTO and ZnO/FTO) revealed considerably lower ratios. At zero bias, the addressed junction demonstrated response/recovery times of 0.175 and 0.178 sec., respectively.

http://doi.org/10.22401/ANJS.28.3.14
*Corresponding author: albeaty33@kus.edu.iq

1. Introduction

UV optoelectronics based nanostructured semiconductors, with efficient figure-of-merits profiles, are considered highly pertinent for wide-reaching applications including space research, optical communication, missile detection, chemical and biological analysis and environmental monitoring [1-3]. However, technology-based nanostructured semiconductors, in precise terms "UV photodetectors", demands succeeding advancement within the confined importance of a number of facilities such as high UV sensitivity, efficiency, sound time-resolved characteristics, visible-spectrum rejection, as well as relatively small driving force consumption so-called self-driven character [4-6]. Particularly, there are binary photo-detecting frameworks which are the photo-conductive and photo-voltaic singularities, wherein the latter includes p–i–n/p–n homo- and/or hetero-junction as well as Schottky photodetectors. Such devices utilize the built-in electric field for the photo-generated electrons/holes separation phenomenon which in turn allows light signal detection even at relatively low driving voltage (bias condition)[7,8]. In this context, varies nanostructured metal oxide semiconductors are being investigated to advance the addressed technology; these include tin oxide (SnO2), zinc oxide (ZnO), germanium dioxide (GeO2), titanium dioxide (TiO2), nickel-oxide (NiO), etc. [9-12]. Among these, NiO has demonstrated wide-reaching applications such as functional layer semiconductor in chemical sensor, electrochromic devices, transparent conductive films, and UV optoelectronics. Additionally, NiO usually demonstrates p-type conductivity along relatively wide room temperature optical bandgap (3.6 eV); NiO is also well-oriented for easy fabrication process for large scale production [13, 14]. Continuously, nanostructured ZnO, with wide optical band gap of 3.3 eV and n-type conductively, has been widely

considered for practical applications like field effect transistors, nanogenerators, strain sensors, solar cells, light emitting diodes, as well as UV photodetectors [15, 16]. Herein, NiO/ZnO heterojunction could demonstrate a considerable potential for effective visible-blind UV photodetector application. Within this framework, the proposed study aims to demonstrate solution-processed visible-blind NiO/ZnO/FTO heterostructure photodetector via double oriented spray pyrolysis approach. In this work, the microstructural analysis along with the optical analysis were investigated; consequently, these analyses are correlated to the attained photo-responsive evaluation of the fabricated NiO/ZnO/FTO heterojunction photodetector. Fluorine-doped tin oxide (FTO) is a transparent conductive oxide that is commonly used as a substrate in various applications, especially in devices such as solar cells, sensors and detectors.

2. Experimental procedure

In typical process, nickel nitrate hexahydrate ($Ni(NO_3)_2 \cdot 6H_2O$) manufactured by Sigma-Aldrich with molar ratio of 0.4 M was dissolved in deionized water for about 45 minutes where the pH level was maintained at 9 through the addition of NaOH with molarity of 1.25 M until a green homogenous solution was attained. Then, the attained solution was sprayed on pre-heated FTO substrate at 350 °C. The FTO substrate was subjected to pre-multicycle cleaning process using soapy water, acetone, and ethanol in ultrasonic bath and subsequently dried using nitrogen flow. Subsequently, 0.4 M zinc nitrate hexahydrate ($Zn(NO_3)_2 \cdot 6H_2O$) was also dissolved in deionized water for similar period to that of NiO with maintained pH at 7.5. The obtained solution was then sprayed on the top of the pre-deposited NiO at a temperate of 300°C. This was accomplished considering an adequate area to consider the Ag metal contact; Figure 1 presents further details of the deposition process as well as a schematic illustration of the fabricated photodetectors.

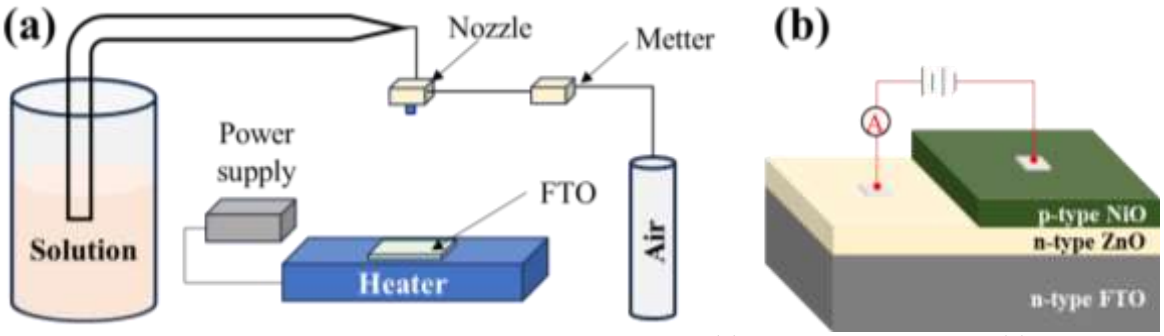

Figure 1. Schematic representation of the proposed work; (a) spray pyrolysis and (b) fabricated NiO/ZnO/FTO.

The microstructural characteristics of the fabricated layers were conducted suing X-ray diffractometer (SHIMADZU, XRD-6000) and Fourier transform infrared spectroscopy (FT-IR, SHIMADZU), while the morphological investigation was carried out using field emission scanning electron microscopy (SU8031, FE-SEM). In the meanwhile, the optical investigation was performed using ultraviolet-visible-infrared light spectroscopy technique (UV-3600, Shimadzu). The photo-responsive evaluation of the fabricated NiO/FTO, ZnO/FTO, and NiO/ZnO/FTO heterojunction using source measure unit (SMU, Keithley 2041) along with optical band-pass filter/s with wavelength ranging from 310 to 808 nm. The current-time profile was investigated based on 10% to 90% of the total attained current over three continuous cycles with pulse width of ≈13 sec.

3. Results and Discussion

The XRD patterns, Figure 2 (a), revealed the occurrence of polycrystalline structure of the deposited films. In detail, ZnO curve mimic a hexagonal structure with reflection angles of 32.05°, 34.68°, 36.53°, 47.78°, 56.85°, 63.12° corresponding to ZnO plans of (100), (022), (101), (102), (110), and (103), respectively; these were found to be in agreement with JCPDS data report no. 05–0669 [17, 18]. In the meanwhile, NiO cubic crystal structure was confirmed through the attainment of XRD plans of (100), (200), and (220) at 2θ ≅ 37.26, 43.28, 62.86,

respectively, which in turn was found to be in good accordance with JCPDS data report no. 04-0835 [19, 20]. The FT-IR spectra elucidated in Figure 2 (b), considering both layers NiO and ZnO, demonstrated O–H stretching between 3200 and 3500 cm^{-1}; another mutual band around 1620 cm^{-1} is due to C=C vibration [21, 22].

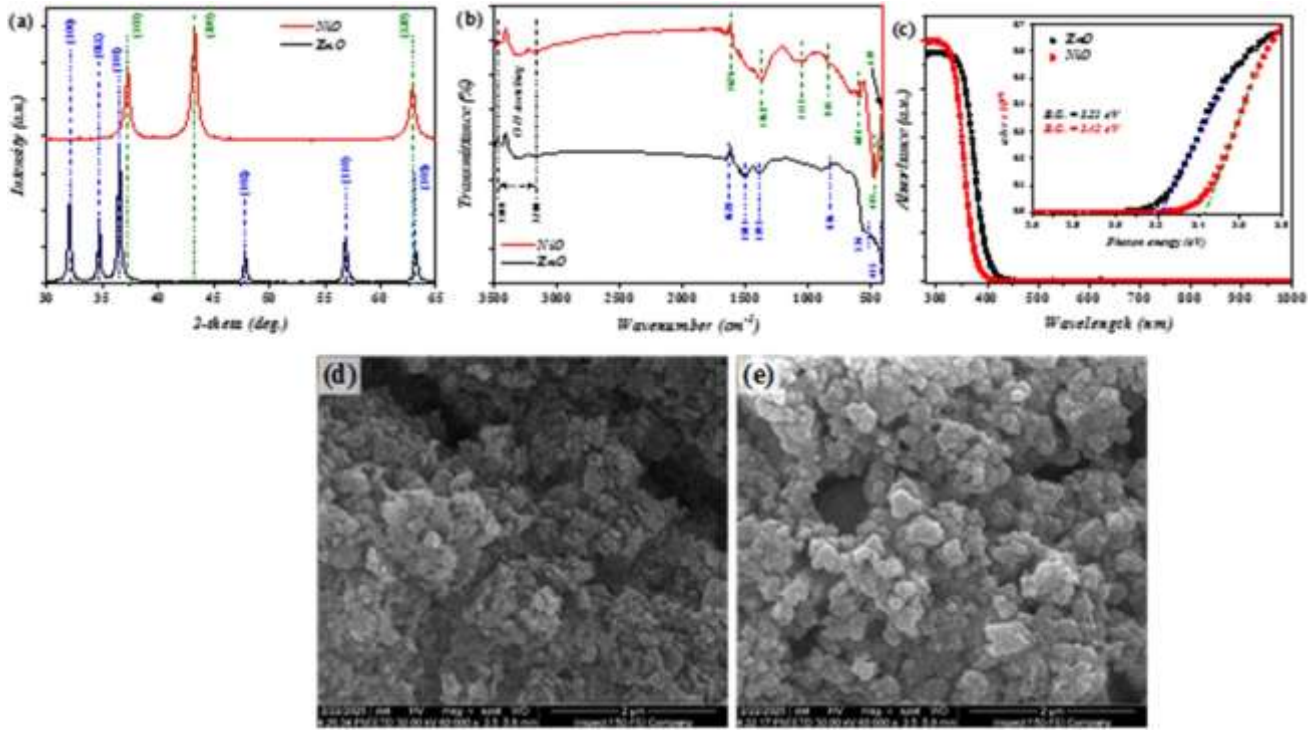

Figure 2. Microstructural characteristics of the deposited film/s; (a) XRD patterns, (b) FT-IR, (c) UV-Vis spectroscopy, while FE-SEM is presented in (d) ZnO and (c) NiO.

In the ZnO spectrum, peaks attained at 1501 and 1393 cm^{-1} are attributed to the C–H and N–H bending, respectively; the metal–oxide (Zn–O) stretching vibrations are located bellow 840 cm^{-1} [23-25]. The absorbance spectra (Figure 2, c) suggest by taking the tangent of the absorbance line towards the x-axis at around 375 and 355 nm for the deposited ZnO and NiO layers, respectively, to determine the optical energy gap. an; this was perceived along with optical band-gaps of 3.21 and 3.42 eV, inset into Figure 2 (c). This was estimated in accordance with the well-known Tauc relation [26-28]. Continuously, the topography analysis (Figure 2, d and e) revealed compact and surface with relatively uniformly agglomerated nanoparticles' films along 2 µm scanned area; this phenomenon was noticed along average nanoparticle diameters of 42.5 and 64.17 nm for ZnO and NiO, respectively. Figure 3 (a-c) represents the attained current-voltage (I-V) characteristics of the fabricated deices under both dark and multi-intensity light (375 nm) episodes wherein non-liner symmetric behavior could be perceived along both reverse and forward bias. Such a phenomenon was further noticed at higher illumination with relatively linear photocurrent (I_{ph}) increment; this was further validated from the I_{ph} profile/s (Figure 1, a and b) with person correlation value close to unity ($R^2 \approx 1$), this indicates the fitting quality of the measured data [29]. In term of the demonstrated junctions, it was noticed that NiO/ZnO heterojunction exhibited higher I_{ph} profile as compared to that of pristine ZnO/FTO and NiO/FTO.

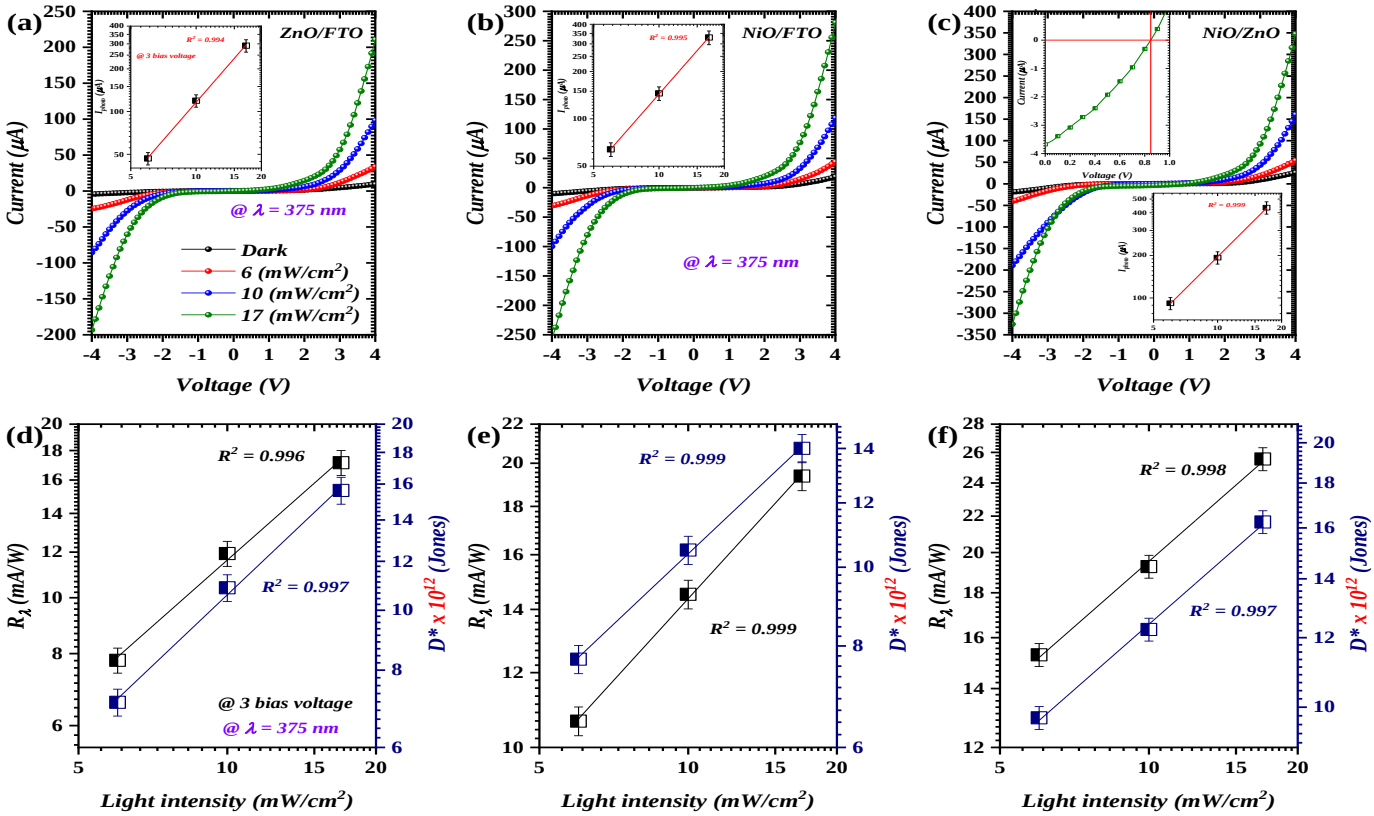

Figure 3. Current-Voltage characteristics of (a) ZnO/FTO, (b) NiO/FTO, and (c) NiO/ZnO with inset showing the self-driven character of NiO/ZnO heterostructure; while the attained figure-of-merits are presented in (d) ZnO/FTO, (e) NiO/FTO, and (f) NiO/ZnO.

The I_{ph} to I_D (dark current) ratio of the fabricated devices revealed values of 340, 304, and 355 for ZnO/FTO, NiO/FTO, NiO/ZnO, respectively. This in turn validates the active role of the utilized layer/s in the generation/recombination of electron/hole pairs within the formed junction [30]. Further, inset into Figure 3 (c) elucidates an independent I-V curve along short-circuit current and open-circuit voltage of 4 μA and 0.8 V indicating the ability of the proposed junction to work in self-driven mode under 375 nm light intensity of 17 mW/cm². Continuously, the figure-of-merits, including photo-responsivity ($R_\lambda = I_{Photo}/P_{in}$) and photo-detectivity ($D^* = R_\lambda A/(2qI_{dark})^{1/2}$) were also considered for the fabricated devices [31, 32]; herein q is electron charge and A is the working area of the device. In general observation, regardless of the junction considered, the investigated figure-of-merits exhibited increasing behavior as a function of the incident light intensity (Figure 3, d-f) along $R^2 \approx 0.99$. In detail, NiO/ZnO heterojunction demonstrated increasing R_λ values from 15.3 to 25.6 mA/W under light intensity of 6 and 17 mW/cm2, respectively; at the pronounced light intensities, the inspected D* delivered values as high as 9.7×10^{12} and 16.3×10^{12} Jones, respectively. The addressed figure-of-merits were found to be considerably lower for pristine ZnO/FTO and NiO/FTO devices which particularize an outstanding ability of light-trapping of the proposed NiO/ZnO heterojunction photodetector. It is worth mentioning that the FTO substrate, in case NiO/ZnO device, is floating and does not contribute directly in the formed junction. However, the substrate could play a crucial role in the photomultiplication singularity which affects the overall device performance [33, 34]. Figure 4 (a-c) depicts the figure-of-merits of the fabricated devices as a function of spectral response. Both fabricated ZnO/FTO and NiO/FTO devices exhibited peak Rλ and D* at wavelength of 375 nm and 340 nm, respectively; such an observation could be mainly due to the presented optical bandgaps of the presented devices, the cut-off wavelength, (Figure2,c).

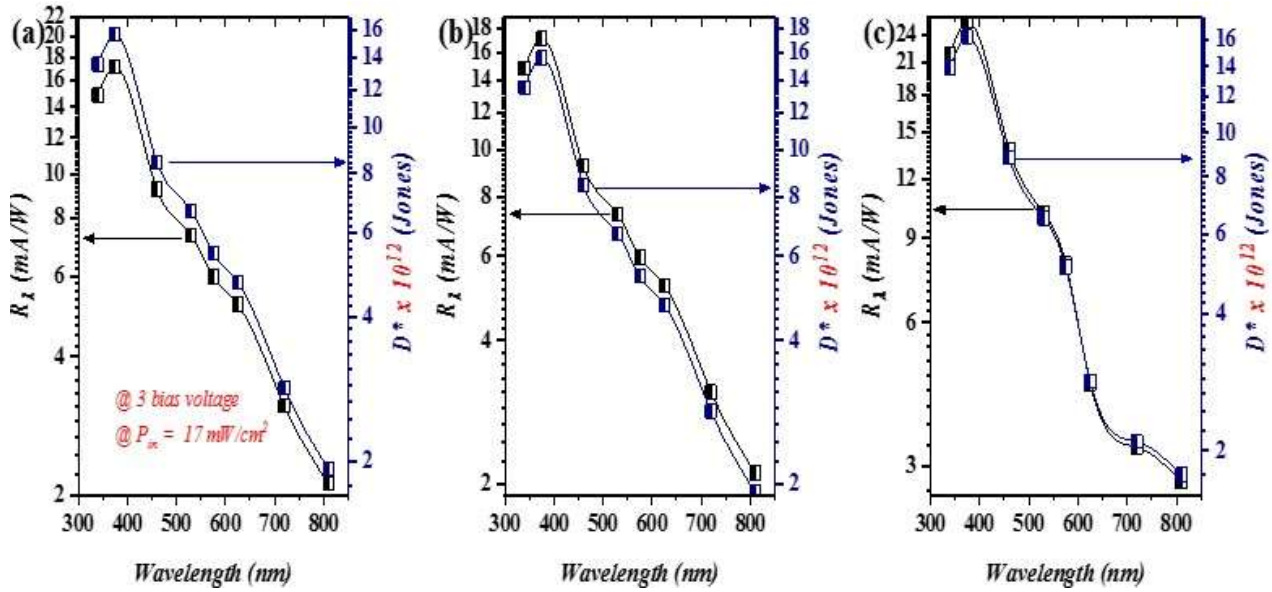

Figure 4. Figure-of-merits including Rλ and D* for (a) ZnO/FTO, (b) NiO/FTO, and (c) NiO/ZnO.

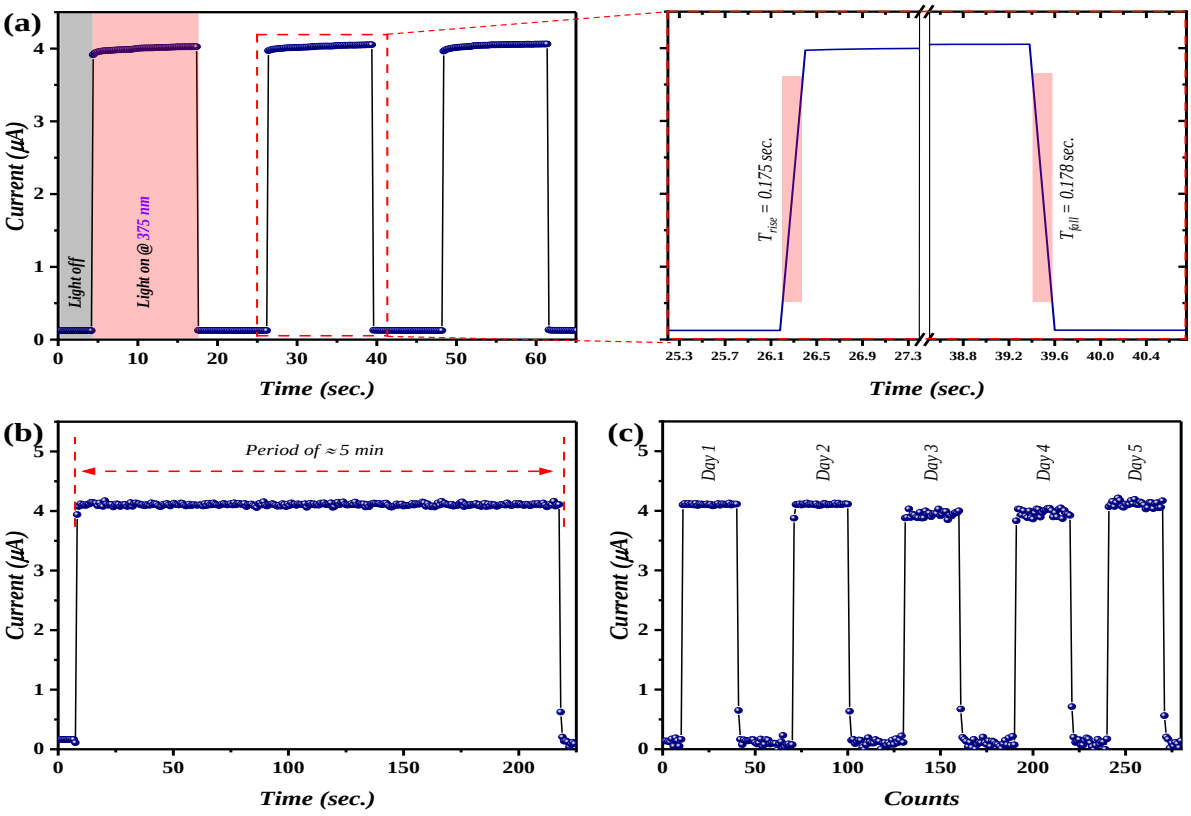

Figure 5. Current-Voltage characteristics of (a) ZnO/FTO, (b) NiO/FTO, and (c) NiO/ZnO with inset showing the self-driven character of NiO/ZnO heterostructure; while the attained figure-of-merits are presented in (d) ZnO/FTO, (e) NiO/FTO, and (f) NiO/ZnO.

Subsequently, the proposed heterojunction, NiO/ZnO, revealed the occurrence of higher values to those of pristine devices with peak Rλ and D* values of 25.6 mA/W and 16.3 $\times 10^{12}$ Jones, respectively. This behavior was found to be considerably decreased as the wavelength approaches the visible region of the scanned spectrum along a rejection ratio ($\lambda_{375}/\lambda_{625}$) of 572 which indicates the visible-blind feature of the proposed geometry; pristine devices demonstrated rejection ratio ($\lambda_{375}/\lambda_{625}$) of 330 and 371, respectively. Figure 5 (a-c) reveals the time-dependent behavior of the proposed self-driven NiO/ZnO heterostructure. The investigated profile revealed rather fast response I_{ph} episode under 375 nm incident light from 0.13 μA (dark state) until the device reached stability at 4.2 μA (illuminated state). This phenomenon was perceived over three multiple cycles along pulse width of ≈13 sec. Such investigation was considered at zero bias voltage which strongly suggest the self-driven feature of the proposed heterojunction. The investigated device delivered rather fast response and recovery behavior over the scanned period of time. In detail, the rise/recovery time of the fabricated heterostructure delivered value of 0.175 and 0.178 sec., respectively. This in turn suggests slightly higher electron/hole generation rate as compare to that of recombination [35-37]. The stability of the NiO/ZnO photodetector was further tested over long illumination run for a period of ≈5 minutes (Figure 5, b). Additionally, the time-dependent characteristic was also demonstrated over a period of five days (Figure 5, c). The stated investigates demonstrated highly stable and robustness device [38]. We were obtained at 17 mW/cm2; a linear I_{ph} to incident wavelength intensity with $R^2 \approx 1$ was also acquired. Further, a decreasing trend in the R_λ profile was perceived as the applied wavelength increased from UV to visible region with $\lambda_{375}/\lambda_{625}$ rejection ratio of 572. The time-resolved characteristics demonstrated rise/fall periods of 0.175 and 0.178 sec., respectively. This was attained along stable switching behavior along five days [39, 40].

Conclusions

Solution-processed NiO/ZnO/FTO heterojunction structure was successfully demonstrated for self-driven visible-blind photodetector application. The intended geometry exhibited considerably photo-responsive characteristics under 375 nm illumination wavelength. In detail, a short-circuit current and an open-circuit voltage of 4 μA and 0.8 V were obtained at 17 mW/cm^2; a linear I_{ph} to incident wavelength intensity with $R^2 \approx 1$ was which has been obtained Further, a decreasing trend in the R_λ profile was perceived as the applied wavelength increased from UV to visible region with $\lambda_{375}/\lambda_{625}$ rejection ratio of 572. The time-resolved haracteristics demonstrated rise/fall periods of 0.175 and 0.178 sec., respectively. This was attained along stable switching behavior along five days.

Acknowledgments: The authors would like to thank the logistic support provided by College of Energy and Environmental Sciences, Al-Karkh University of Science.

Conflict of Interest: Authors declare no conflict of interest pertaining this work.

Funding: No funding is received for this work.

Reference

[1] Aldaghri, O.; Salih, E.Y.; Ramizy, A., Mohammed, A.S.; Ibnaouf, K.H.; Eisa, M.H.; "Rapid fabrication of fast response CdS/Si visible light photodetector: Influence of laser energy". Results in Physics, 54: 107112, 2023.

[2] Ahmed, D.S.; Mohammed, M.K.; "Novel mixed solution of ethanol/MACl for improving the crystallinity of air-processed triple cation perovskite solar cells". Solar Energy, 207: 1240-6, 2020.

[3] Salim, E.T.; Fakhri, M.A.; Tariq, S.M.; Azzahrani, A.S.; Ibrahim, R.K.; Alwahib, A.A.; et al. "The unclad single-mode fiber-optic sensor simulation for localized surface plasmon resonance sensing based on silver nanoparticles embedded coating". Plasmonics, 19: 131-43, 2024.

[4] Ghlem, M.A.H.; Ahmed, M.A.; Dhahir, A.K.A.; Al-Khafaji, T.K.M.S.; Thamer, S.A.; "Room temperature NO2 gas sensor based mesoporous Zn/Al-layered double hydroxide". The effect of molar ratio. Materials Letters, 376: 137280, 2024.

[5] Al-Taa'y, W.A.; Al-Beayaty, MA.H.; Abbas, L.J.; "Microstructural and Mechanical Properties Study of Al/SiC composite prepared by PM technique". Iraqi Journal of Science, 459-68, 2025.

[6] Ahmed, D.S.; Mohammed, M.R.; Mohammed, M.K.; "Synthesis of multi-walled carbon nanotubes decorated with ZnO/Ag nanoparticles by co-precipitation method". Nanoscience & Nanotechnology-Asia, 10:127-33, 2020.

[7] Mohammed, M.K.; "Studying the structural, morphological, optical, and electrical properties

of CdS/PbS thin films for photovoltaic applications". Plasmonics, 15:1989-96, 2020.
[8] Bashir, M.B.A.; Salih, E.Y.; Rajpar, A.H.; Bahmanrokh, G.; Sabri, M.F.M.; "The impact of laser energy on the photoresponsive characteristics of CdO/Si visible light photodetector". Journal of Micromechanics and Microengineering, 32: 085006, 2022.
[9] Al-Beayaty,M.A.H.; Abbas, L.K.; "Mohammed RK. Effect of L-cysteine capping the CdSe, CdSe: CdS on structural and morphological properties". AIP Conference Proceedings: AIP Publishing, 2023.
[10] Salih, E.Y.; "Fabrication and photodetection performance evaluation of nanostructured CdS/Si MSM visible light photodetector". Optical Materials, 149:115120, 2024.
[11] Salih, E.; Ramiz, y.A.; Aldaghr, i.O.; Eisa, M.H.; Ibnaouf, K.H.; "Solution processed self-powered broadband flower-like Zn (Al) O-mixed metal oxide dye sensitized photodetector". Materials Letters, 362:136213, 2024.
[12] Abdulghani, S.O.; Salih, E.Y.; Mohammed, A.S.; "Fabrication and photo-responsive characteristics of GeO2 doped SnO2/porous Si film for ultraviolet photodetector application". Materials Chemistry and Physics, 303:127859, 2023.
[13] Mohammed, A.S.; Fahad, O.A.; Ramizy, A.; Salih, E.Y.; "Thickness effect of Al2O3 as buffer layer on Alq3 sensitivity for toxic gas". Ceramics International, 47:17907-14, 2021.
[14] Salleh, F.; Usop, R.; Saugi, N.S.; Salih, E.Y.; Mohamad, M.; Ikeda, H.; et al. "Influence of TiO2 layer's nanostructure on its thermoelectric power factor". Applied Surface Science, 497:143736, 2019.
[15] Klochko, N.; Kopach, V.; Tyukhov, I.; Zhadan, D.; Klepikova, K.; Khrypunov, G.; et al. "Metal oxide heterojunction (NiO/ZnO) prepared by low temperature solution growth for UV-photodetector and semi-transparent solar cell. Solar Energy". 164:149-59,2018.
[16] Al-Beayaty, M.A.H.; "Structural, optical and morphological characterization of Cdse/Cds Core/shell quantum dots synthesized via chemical bath". Iraqi Journal of Science, 4323-32, 2021.
[17] Debnath, R.; Xie, T.; Wen, B.; Li, W.; Ha, JY.; Sullivan, NF.; et al. "A solution-processed high-efficiency p-NiO/n-ZnO heterojunction photodetector". Rsc Advances, 5:14646-52, 2015.
[18] Bashir, M.B.A.; Said, S.M.; Sabri, M.F.M.; Miyazaki, Y.; Shnawah, D.A.; Shimada, M,; et al. "In-filled La 0.5 Co 4 Sb 12 skutterudite system with high thermoelectric figure of meri"t. Journal of Electronic Materials, 47:2429-38, 2018.
[19] Salih, E.Y.; Sabri, M.F.M.; Sulaiman, K.; Hussein, M.Z.; Said, S.M.; Usop, R.; et al. "Thermal, structural, textural and optical properties of ZnO/ZnAl2O4 mixed metal oxide-based Zn/Al layered double hydroxide". Materials Research Express, 5:116202, 2018.
[20] Salih, E.Y.; Ramizy, A.; Aldaghri, O.; Mohd Sabri, M.F.; Madkhali, N.; Alinad, T.; et al. "In-depth optical analysis of Zn (Al) O mixed metal oxide film-based Zn/Al-layered double hydroxide for TCO application". Crystals, 12:79, 2022.
[21] Salih, E.Y.; Abbas, Z.; Al Ali, S.H.H.; Hussein M.Z.; "Dielectric behaviour of Zn/Al-NO 3 LDHs filled with polyvinyl chloride composite at low microwave frequencies". Advances in Materials Science and Engineering, 2014, 2014.
[22] Mohammad, M.R.; Ahmed, D.S.; Mohammed, M.K.; "ZnO/Ag nanoparticle-decorated single-walled carbon nanotubes (SWCNTs) and their propertie". Surface Review and Letters, 27:1950123, 2020.
[23] Salih, E.Y.; Bashir, M.B.A.; Rajpar, A.H.; Badruddin, I.A.; Bahmanrokh, G.; "Rapid fabrication of NiO/porous Si film for ultra-violate photodetector: The effect of laser energy". Microelectronic Engineering, 258:111758, 2022.
[24] Patel, M.; Kim, J.; "Transparent NiO/ZnO heterojunction for ultra-performing zero-bias ultraviolet photodetector on plastic substrate". Journal of Alloys and Compounds, 729:796-801, 2017.
[25] Mohammed,Salam,A.;Hasan, Ali.; Al-Taa'y, Wasan.A.; Ahmed, Ahmed.; Khalaf, Maji.; ; Yousif, Emad.;" Optical properties Study of New Films Derived from poly(vinyl chloride)- N-(4-Hydroxy-phenyl)-acetamide". Research Journal of Pharmaceutical, Biological and Chemical Sciences, 7(Issue 4) :1064 - 1071, 2016.
[26] Dinesh, V.P.; Biji, P.; Kumaravel, M.; Tyagi, A.; Kamaruddin, M.; "Synthesis and characterization of hybrid ZnO@ Ag core-shell nanospheres for gas sensor applications". Materials Science Forum: Trans Tech Pub, 768-73, 2012.
[27] Nalage, S.; Navale, S.; Patil, V.; "Polypyrrole-NiO hybrid nanocomposite: structural, morphological, optical and electrical transport studies". Measurement, 46:3268-75, 2013.
[28] Al-Taa'y, Wasan.A.; Hasan, Bushra. A.;" Design and Fabrication of Nanostructure TiO2 Doped NiO as A Gas Sensor for NO2 Detection". Iraqi

Journal of Science, 62 (Issue 11): 4385 - 439625, 2021

[29] Drozdowska, K.; Welearegay, T.; Österlund, L.; Smulko, J.; "Combined chemoresistive and in situ FTIR spectroscopy study of nanoporous NiO films for light-activated nitrogen dioxide and acetone gas sensing". Sensors and Actuators B: Chemical, 353:131125, 2022.

[30] Vivek, C.; Balraj, B.; Thangavel, S.; "Structural, optical and electrical behavior of ZnO@ Ag core–shell nanocomposite synthesized via novel plasmon-green mediated approach". Journal of Materials Science: Materials in Electronics, 30:11220-30, 2019.

[31] Mohammed, M.K.; Al-Mousoi, A.K.; Khalaf, H.A.;. "Deposition of multi-layer graphene (MLG) film on glass slide by flame synthesis technique". Optik,127:9848-52, 2016.

[32] Bashir, M.B.A.; Salih, E.Y.; Sabri, M.F.M.; "Rajpar AH, Badruddin IA, Hussein MZ, et al. In-depth thermal, microstructural and photoluminescence analysis of mesoporous ZnO/ZnAl2O4-MMO: the effect of molar ratio". ECS Journal of Solid State Science and Technology, 10:106006 ,2021.

[33] Mohammed M.K.; Naji, A.M.; Ahmed, D.S.; Jamai, M.J.; Salih, E.Y,; Dehghanipour, M.; et al. "Facile synthesis of chitosan-MoS2 over reduced graphene oxide to improve photocatalytic degradation of methylene blu"e. Journal of Sol-Gel Science and Technology,1-11, 2024.

[34] Salih, E.Y.; "Characterization and performance evaluation of nanostructured rod-like CdTe/Si fast-response visible light photodetector". Physica B: Condensed Matter, 685:416056, 2024.

[35] Salih, E.;"Opto-electrical evaluation of visible blind fast-response nanostructured SnO 2/Si photodetector". RSC advances., 14:27733-40, 2024.

[36] Huang, Z.; Zhou ,Y.; Luo, Z.; Yang, Y.; Yang, M.; Gao, W.; et al. "Integration of photovoltaic and photogating effects in a WSe 2/WS 2/p-Si dual junction photodetector featuring high-sensitivity and fast-response". Nanoscale Advances, 5:675-84, 2023.

[37] Ghosh, C.; Dey, A.; Biswas, I.; Gupta, R.K.; Yadav, V.S.; Yadav, A.; et al. "CuO–TiO2 based self-powered broad band photodetector". Nano Materials Science, 6:345-54, 2024.

[38] Salih, E.Y.; "Fabrication of CdSe/Si nanostructure for self-powered visible light photodetector". Materials Letters, 371:136930, 2024.

[39] Yu, S.H.; Lee, Y.; Jang, S.K.; Kang, J.; Jeon, J,.; Lee, C.; et al. "Dye-sensitized MoS2 photodetector with enhanced spectral photoresponse". ACS nano, 8:8285-91, 2014.

[40] Lee,Y.;Yu, S.H.; Jeon,J.; Kim, H.; Lee,.J.Y.; Kim,H.;et al. "Hybrid structures of organic dye and graphene for ultrahigh gain photodetectors". carbon. 88:165-72, 2015.